JCI insight

RESEARCH ARTICLE

Myeloid folliculin balances mTOR activation to maintain innate immunity homeostasis

Jia Li,[1,2] Shogo Wada,[1] Lehn K. Weaver,[3] Chhanda Biswas,[3] Edward M. Behrens,[3] and Zoltan Arany[1]

[1]Department of Medicine, Cardiovascular Institute, Perelman School of Medicine, University of Pennsylvania, Philadelphia, Pennsylvania, USA. [2]Department of Aerospace Medicine, Fourth Military Medical University, Xi'an, China. [3]Department of Pediatrics, Division of Rheumatology, Children's Hospital of Philadelphia, Philadelphia, Pennsylvania, USA

The mTOR pathway is central to most cells. How mTOR is activated in macrophages and how it modulates macrophage physiology remain poorly understood. The tumor suppressor folliculin (FLCN) is a GAP for RagC/D, a regulator of mTOR. We show here that LPS potently suppresses FLCN in macrophages, allowing nuclear translocation of the transcription factor TFE3, leading to lysosome biogenesis, cytokine production, and hypersensitivity to inflammatory signals. Nuclear TFE3 additionally activates a transcriptional RagD-positive feedback loop that stimulates FLCN-independent canonical mTOR signaling to S6K and increases cellular proliferation. LPS thus simultaneously suppresses the TFE3 arm and activates the S6K arm of mTOR. In vivo, mice lacking myeloid FLCN reveal chronic macrophage activation, leading to profound histiocytic infiltration and tissue disruption, with hallmarks of human histiocytic syndromes, such as Erdheim-Chester disease. Our data thus identify a critical FLCN-mTOR-TFE3 axis in myeloid cells, modulated by LPS, that balances mTOR activation and curbs innate immune responses.

Introduction

The mTOR complex 1 (mTORC1) is a central kinase complex that senses ambient nutrient status to determine cell behavior via phosphorylation of various downstream substrates (1). Despite of the important role of mTORC1, its detailed function in innate immunity has yet to be determined.

In most cells, mTORC1 activity is highly sensitive to nutrient status, in particular the presence of amino acids (2–4). A lysosome-associated machinery, comprising v-ATPase, Ragulator complex, and Rag GTPases, is essential for amino acid sensing and subsequent mTORC1 activation (5). When the intracellular amino acid level is sufficient, Rag GTPases directly bind and recruit mTORC1 to the lysosome surface, where Rheb activates mTORC1 (6). Rag GTPases comprise heterodimers of RagA or B, with RagC or D (2). Activity of Rag GTPases is tightly regulated through guanyl nucleotide status of each Rag GTPase component. RagA/B is active while loaded with GTP, while RagC/D is active while loaded with GDP (2). GEFs and GAPs for each Rag GTPase modulate their activity (7, 8). Recently the protein folliculin (FLCN) was identified as a GAP for RagC/D, suggesting that it plays a role in amino acid sensing (9, 10).

FLCN was originally identified as a tumor suppressor gene, mutated in Birt-Hogg-Dube syndrome (11). Loss-of-function mutations of FLCN lead to significant mitochondrial biogenesis and lysosome biogenesis in many cell types (12), although how this transcriptional program was activated remained unclear until recently. Our group recently showed in adipocytes that the transcription factor TFE3 is a dominant downstream mediator of FLCN action (13). TFE3 is a member of the TFE/MiTF bHLH transcription factor family, which includes TFEB, a master regulator of lysosome biogenesis (14). FLCN sequesters TFE3 and possibly other TFE/MiTF members in the cytoplasm upon ambient amino acid availability. Mechanistically FLCN acts as a GAP to RagC/D, promoting its active GDP-bound form (9, 10), which in turn stimulates mTORC1 to phosphorylate a 14-3-3–binding motif of TFE3, thereby leading to its cytoplasmic retention (13, 15, 16). Interestingly, however, while loss of FLCN abrogates TFE3 phosphorylation, loss of FLCN does not affect phosphorylation status of other canonical mTORC1 sub-

Authorship note: JL, SW, and LKW contributed equally to this work.

Conflict of interest: The authors have declared that no conflict of interest exists.

Submitted: December 18, 2018
Accepted: February 11, 2019
Published: March 21, 2019.

Reference information: JCI Insight. 2019;4(6):e126939. https://doi.org/10.1172/jci.insight.126939.

strates (e.g., S6K1), indicating that FLCN modulates mTORC1 substrate specificity. In fact, in numerous contexts FLCN deletion induces higher canonical mTORC1 activity, leading to hyperproliferation and tumorigenesis (17–20). The mechanism by which canonical mTORC1 signaling is activated in the absence of FLCN is not known.

In this study, we investigate the role of FLCN in myeloid cells, reasoning that specific activation of mitochondrial and lysosomal biogenesis would affect both proliferation and immune activation of these cells. We show that LPS suppresses FLCN expression, leading to hypersensitive inflammatory responses in cell culture and in vivo, and that these responses are mediated via TFE3. Moreover, we identify a TFE3-mediated feedback loop that explains canonical mTORC1 activation when FLCN is deleted. This study thus identifies a FLCN-TFE3 axis that connects immune responses and canonical and noncanonical mTORC1 activities in myeloid cells.

Results

FLCN deletion in myeloid/macrophage cell lineage leads to constitutive activation of TFE3. To test the role of FLCN in myeloid cells/macrophages, a lentiviral CRISPR-Cas9 system was used to generate genome-edited RAW 264.7 mouse macrophage cells with endogenous FLCN KO (Figure 1A). In the absence of FLCN, the phosphorylation of TFE3 at Ser320 was abolished (Figure 1A), as seen in other cell types (13). Consistent with absence of Ser320 phosphorylation, which is required for cytoplasmic retention of TFE3, TFE3 localized to the nuclei in FLCN-KO cells (Figure 1B), and target genes encoding for lysosome proteins were induced (Figure 1C). To test if similar observations would be made in primary cells, rather than immortalized cells, we cultured bone marrow–derived macrophages (BMDMs) from $FLCN^{lox/lox}$ Lyz2 Cre mice (FLCN myeloid KO mice) versus littermate controls. KO efficiency of FLCN, confirmed by qPCR, was nearly 90%, and gene expression of GPNMB, a canonical TFE3 target gene (21), was markedly increased in FLCN-KO BMDMs (Figure 1D). Immunofluorescence staining of endogenous TFE3 showed strong nuclear localization following FLCN deletion (Figure 1E), and lentiviral ectopic expression of FLCN rescued the cytoplasmic retention of TFE3 (Figure 1F). Lysosomal genes, including *Lamp1*, *Ctsz*, *Ctsd*, *Mcoln1*, *Tpp1*, and *Clcn7*, known to be regulated by TFE3 (22), were induced by 1.5-fold to 3.5-fold in FLCN-deleted BMDMs compared with WT control cells, and lysosomal biogenesis was strongly induced, as shown by immunofluorescence staining of LAMP2 (Figure 1, G and H). Collectively, these data thus show that FLCN promotes cytoplasmic retention of TFE3 in macrophages, inhibiting the ability of TFE3 to activate its target lysosomal genes.

LPS but not CpG suppresses FLCN, which mediates TFE3 nuclear localization. TFE3 and TFEB translocate to nuclei upon LPS stimulation (23), but how LPS mediates TFE3 nuclear localization is not known. We treated BMDMs with LPS, as well as CpG, mimicking bacterial DNA stimulation, for 24 hours. Interestingly, LPS induced a time-dependent suppression of FLCN in BMDMs, resulting in a 90% loss of FLCN at the 24-hour time point, while CpG treatment showed no effects on FLCN expression (Figure 2A). Treatment with a number of additional TLR agonists, including Poly I:C (TLR3), Pam3CSK4 (TLR1/2), and R848 (TLR7/8), demonstrated that LPS (TLR4) has the most profound effect on FLCN expression (Supplemental Figure 1A; supplemental material available online with this article; https://doi.org/10.1172/jci.insight.126939DS1), implying a largely specific effect of TLR4 activation. Interestingly, LPS stimulation did not alter the mRNA expression of FLCN, indicating that the regulation of FLCN occurs at the protein level (Supplemental Figure 1B). Moreover, treatment with the proteasome inhibitor MG132 only partially rescued LPS-induced FLCN protein suppression (Supplemental Figure 1C), indicating some, but a relatively minor, role for the proteasome in regulating FLCN protein stability.

Consistent with the above findings, LPS, but not CpG treatment, resulted in nearly 85% nuclear translocation of TFE3, despite, in both cases, the adoption of a spread out morphology, with membrane projections indicative of activated status (Figure 2B). TFE3 Ser320 phosphorylation was dramatically reduced in LPS-treated cells (Figure 2C, top), the timing of which coincided with TFE3 being found in nuclear fractions (Figure 2C, bottom), while CpG, if anything, had the opposite effects. Treatment with the mTOR inhibitor Torin-1 mimicked the effect of LPS (Figure 2C). Finally, and importantly, ectopic expression of doxycycline-inducible FLCN-HA in BMDMs exposed to LPS completely prevented translocation of TFE3 to the nucleus, even after 24 hours of stimulation (Figure 2D). Taken together, these data demonstrate that LPS promotes nuclear translocation of TFE3 via suppression of FLCN/mTOR-mediated phosphorylation of TFE3.

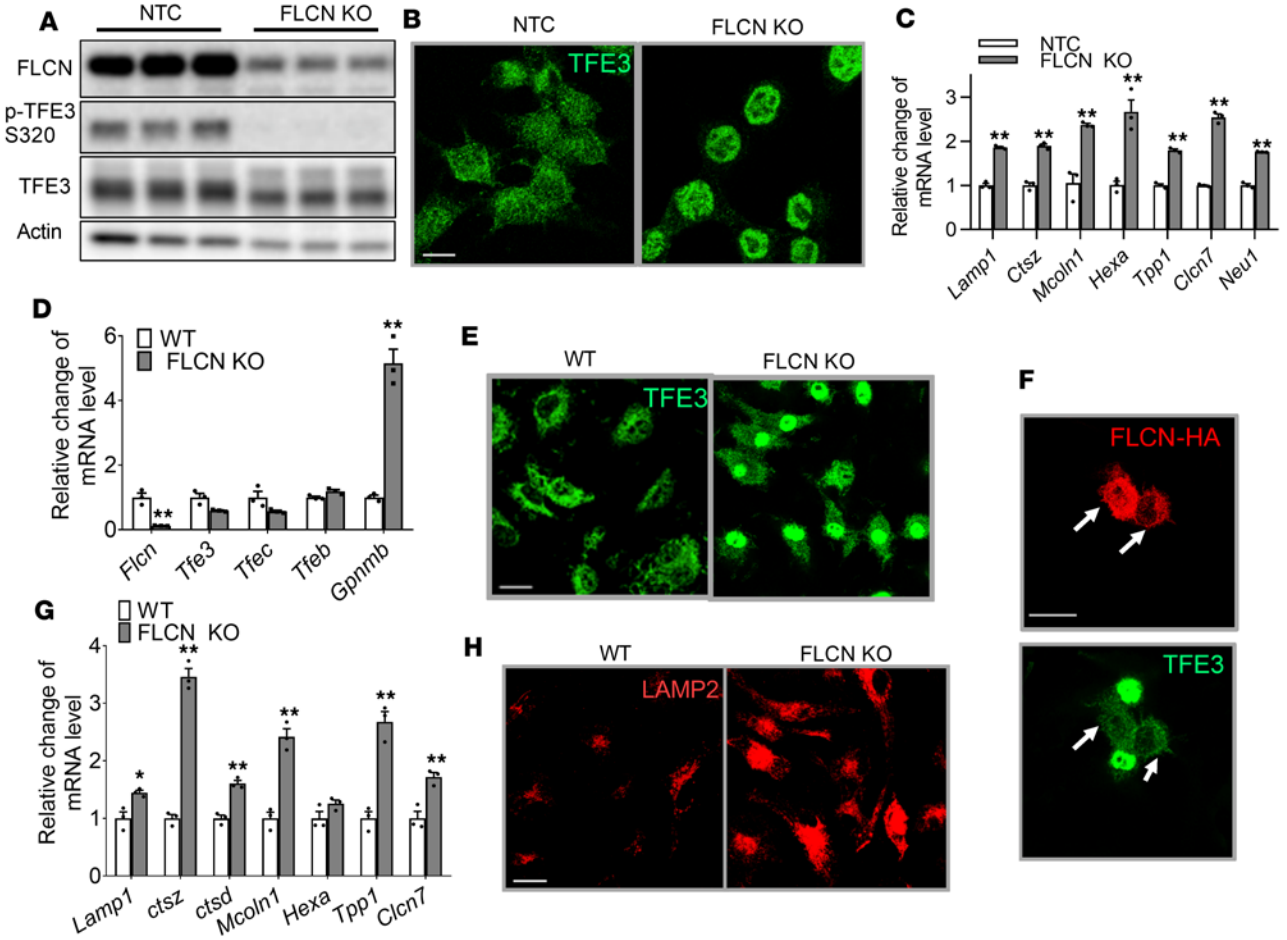

Figure 1. FLCN deletion in myeloid/macrophage cell lineage leads to constitutive activation of TFE3. (**A**) Western blot of FLCN, phospho-TFE3 (Ser320), and TFE3 in the FLCN-KO and nontarget control (NTC) RAW 264.7 cells. (**B**) Immunofluorescence staining of TFE3 (green) in the FLCN-KO and NTC RAW 264.7 cells. (**C**) Relative mRNA expression in the FLCN-KO and NTC RAW 264.7 cells was quantified by quantitative reverse transcription–PCR (qRT-PCR). The data were normalized to a reference gene, 36B4. Values are represented as mean ± SEM from 3 independent experiments. $^{**}P < 0.01$ vs. NTC, determined by Student's *t* test. (**D**) Relative mRNA expression in primary cultured bone marrow–derived macrophages (BMDMs) isolated from $FLCN^{lox/lox}$ mice (WT) and $FLCN^{lox/lox}$ Lyz2 Cre mice (FLCN KO). Values are represented as mean ± SEM from 3 independent experiments. $^{**}P < 0.01$ vs. WT, determined by Student's *t* test. (**E**) Immunofluorescence staining of TFE3 (green) in the WT and FLCN-KO BMDMs. Scale bar: 10 μm. (**F**) Immunofluorescence staining of FLCN-HA (red) and TFE3 (green) in the FLCN-KO BMDMs overexpressed by doxycycline-inducible FLCN-HA. TFE3 was distributed in the cytoplasm of cells with successful FLCN-HA transfection (white arrows) but retained in the nuclear of FLCN-deleted BMDMs without transfection. Scale bar: 10 μm. (**G**) Relative mRNA expression of lysosome genes in the WT and FLCN-KO BMDMs. Values are represented as mean ± SEM from 3 independent experiments. $^{*}P < 0.05$, $^{**}P < 0.01$ vs. WT, determined by Student's *t* test. (**H**) Immunofluorescence staining of LAMP2 (red) in the WT and FLCN-KO BMDMs. Scale bar: 10 μm.

TFE3 promotes canonical mTORC1 activity through a transcriptional RagD feedback loop. FLCN is a GAP for RagC/D, promoting its activated GDP-bound state, and RagC/D is required for mTORC1 activity (3, 9). We therefore assessed if the phosphorylation status of canonical mTORC1 substrates is also blunted by FLCN deletion, as is TFE3. Surprisingly, however, p-S6 and p-mTOR levels were increased, rather than decreased, in BMDMs lacking FLCN (Figure 3A, left lanes). Moreover, neither activation of canonical mTOR by LPS nor CpG was affected by FLCN deletion in BMDMs (Figure 3A, middle and right lanes). Importantly, the increase in canonical mTOR was reversed by concomitant deletion of TFE3 (DKO, Figure 3A), indicating the presence of a TFE-mediated feedback loop. To test whether activated TFE3 is sufficient to activate this feedback loop, we ectopically expressed a TFE3 mutant unable to be phosphorylated by mTORC1 (S320A). As expected, TFE3 S320A was constitutively localized in nuclei while WT TFE3 was mostly cytoplasmic (Figure 3B, left). Strikingly, TFE3 S320A was sufficient to strongly induce mTORC1 activity, as evidenced by increased phosphorylation of mTOR (Ser2448) and S6 ribosomal protein (Ser240/244) (Figure 3B, right).

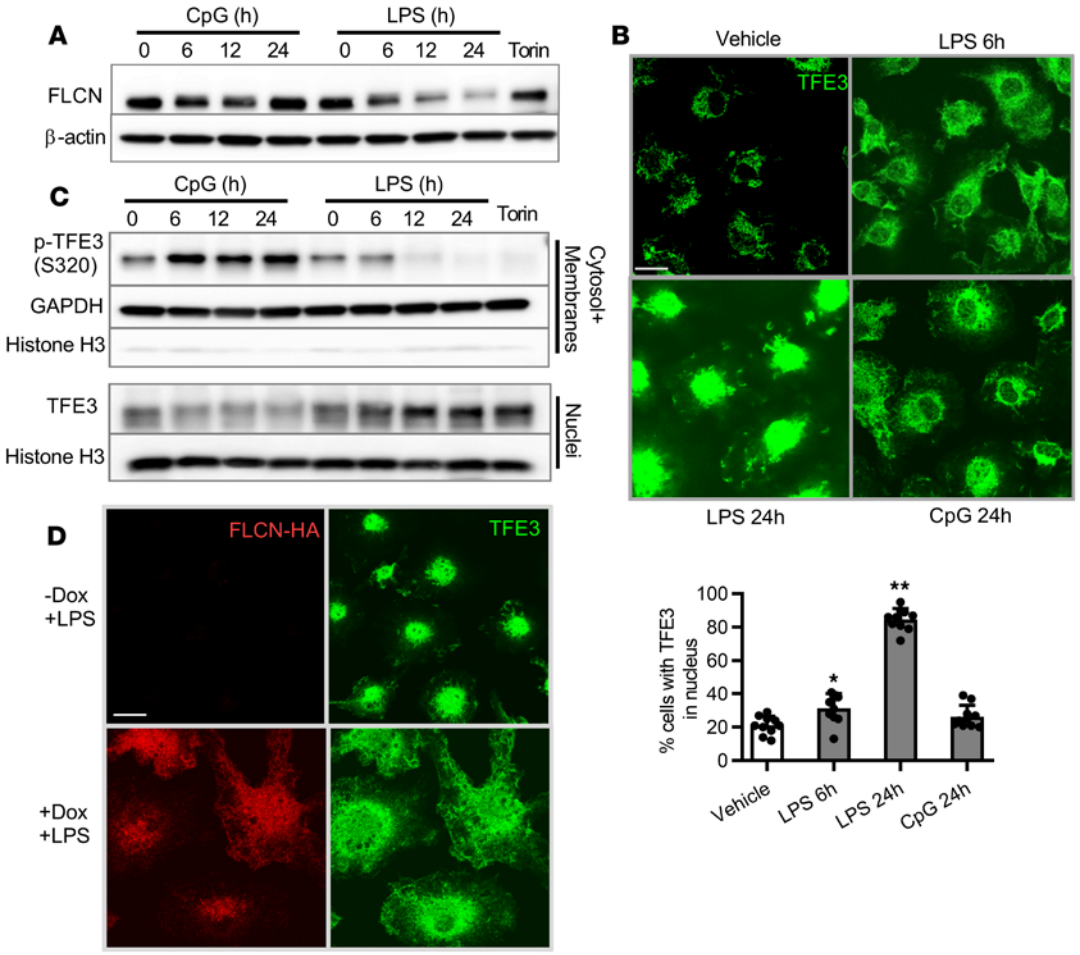

Figure 2. LPS but not CpG suppresses FLCN expression and subsequently induces TFE3 nuclear translocation. (**A**) FLCN expression was determined in BMDMs exposed to CpG (10 μg/ml) or LPS (100 ng/ml) stimulation for 0, 6, 12, and 24 hours. (**B**) Immunofluorescence staining of TFE3 (green) in BMDMs exposed to vehicle, CpG, or LPS stimulation up to 24 hours. Scale bar: 10 μm. The bar graph shows quantification of TFE3 nuclear translocation from **C**. Values are represented as mean ± SEM. $^*P < 0.05$, $^{**}P < 0.01$ vs. vehicle, by 1-way ANOVA followed by *t* test (Bonferroni correction) ($n = 10$, >160 cells per trial). (**C**) Nuclear-cytoplasmic fractionation of phospho-TFE3 (Ser320) and TFE3 expression in BMDMs exposed to CpG or LPS stimulation for 0, 6, 12, and 24 hours. Treatment with the mTOR inhibitor Torin-1 (250 nM) for 3 hour served as a positive control. Histone H3 serves as a specific marker of nuclear fraction. (**D**) Immunofluorescence staining of FLCN-HA (red) and TFE3 (green) in LPS-stimulated BMDMs. Overexpression of doxycycline-inducible FLCN-HA blocked the redistribution of TFE3 from the cytosol to nucleus induced by LPS. DOX, doxycycline (1 μg/ml, 24 hours). Scale bar: 10 μm.

We next interrogated the mechanism by which TFE3 activates the canonical mTORC1 pathway in BMDMs. MiTF/TFE transcription factors have been reported to transcribe RagD to facilitate mTORC1 activity (24). Of all Rag GTPases, RagD was the most strongly induced in BMDMs lacking FLCN, and the induction required the presence of TFE3 (Figure 3C). Moreover, LPS stimulation induced a selective 13-fold increase in RagD mRNA expression, while CpG stimulation showed no effects (Figure 3D). To test the epistatic relationship between FLCN and RagD, we knocked down RagD via siRNA in WT versus FLCN-KO BMDMs. As shown in Figure 3E, siRagD entirely reversed the activation of canonical mTORC1 signaling induced by FLCN loss. Collectively, these data therefore indicate that deletion of FLCN in macrophages selectively prevents mTORC1-mediated suppression of TFE3 and that activation of this TFE3 branch directly leads to a RagD feedback loop that in fact promotes canonical activity of mTOR (Figure 3F).

BMDMs lacking FLCN are hypersensitive to LPS and CpG stimuli. LPS-mediated activation of canonical mTORC1 has been implicated in macrophage inflammatory response (25, 26), and TFE3 and TFEB have recently been shown to drive mRNA expression of inflammatory genes in macrophages (23). We therefore reasoned that cells lacking FLCN, in which both of these pathways are activated, may be partially activated, even in absence of inflammatory stimulation, and/or may be hypersensitive to inflammatory signals. As shown in Figure 4A, BMDMs lacking FLCN exhibited morphological signs of spontaneous activation,

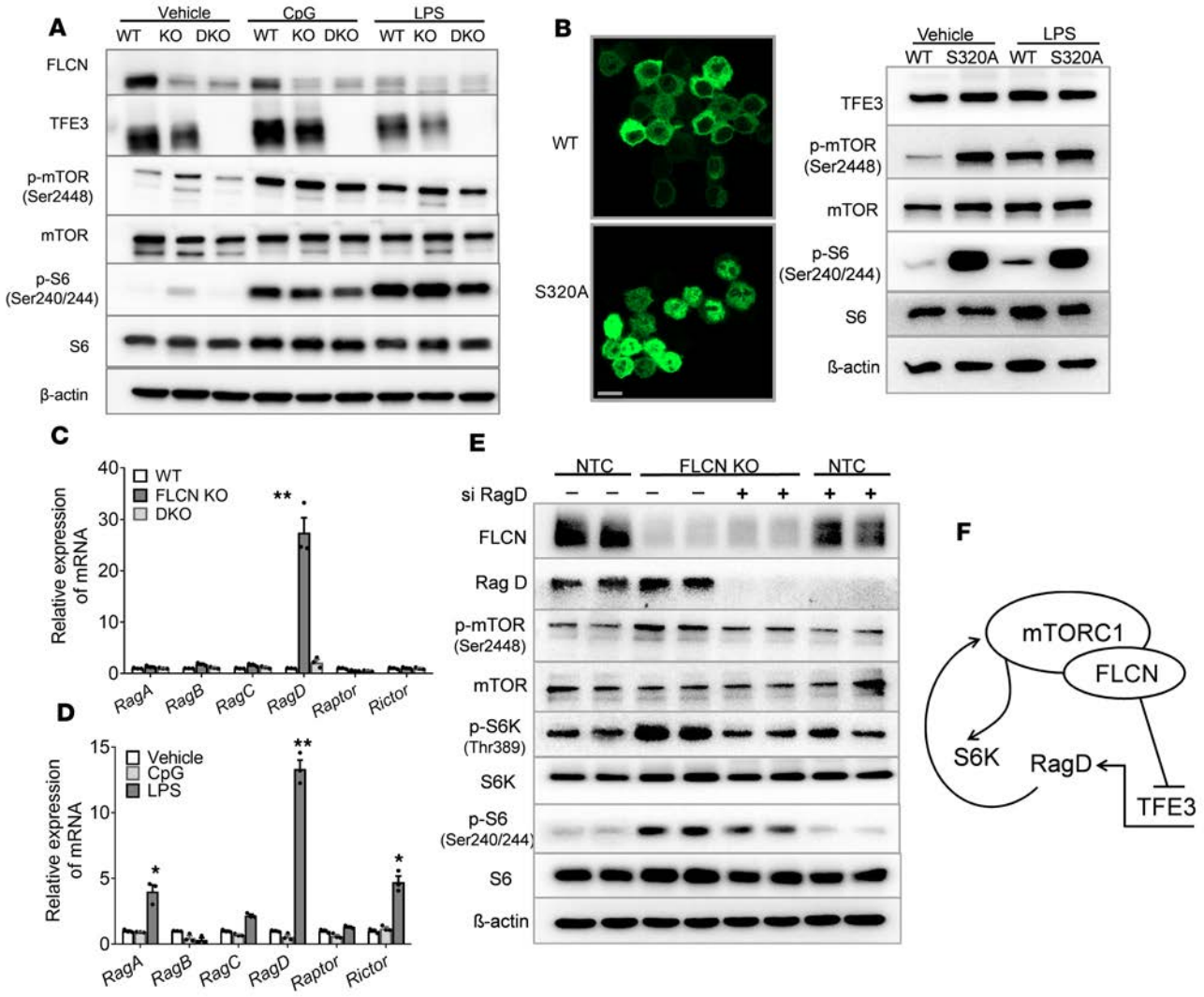

Figure 3. TFE3 promotes canonical mTORC1 activity through a transcriptional RagD feedback loop. (**A**) Western blot of BMDMs isolated from $FLCN^{lox/lox}$ (WT), $FLCN^{lox/lox}$ Lyz2 Cre (FLCN KO [KO]), and $FLCN^{lox/lox}$ Lyz2 Cre TFE3 KO (FLCN and TFE3 double-KO [DKO]) mice exposed to vehicle, CpG (10 μg/ml), or LPS (100 ng/ml) for 24 hours. (**B**) Immunofluorescence staining of TFE3-HA (green) and Western blot of stably expressed WT TFE3 (WT) or mTOR site-mutated TFE3 (S320A) RAW 264.7 cells. LPS (100 ng/ml, 24 hours). Scale bar: 10 μm. p-S6, phospho-S6 ribosomal protein (Ser240/244). (**C**) Relative mRNA expression in WT, FLCN KO, and DKO BMDMs. $^{**}P < 0.01$ vs. WT. (**D**) Relative mRNA expression in the WT BMDMs exposed to vehicle, CpG, or LPS for 24 hours. $^{*}P < 0.05$, $^{**}P < 0.01$ vs. vehicle. (**C** and **D**) Values are represented as mean ± SEM from 3 independent experiments and were analyzed by 1-way ANOVA followed by *t* test (Bonferroni correction). (**E**) BMDMs transfected with a lentiviral CRISPR-Cas9 FLCN KO (FLCN KO) or nontarget control (NTC) on day 1 after isolation and then transfected with RagD siRNA or siControl on day 7. Western blot was performed on day 9 after isolation. (**F**) Proposed models of FLCN-mTOR-TFE3 axis in myeloid cells.

including loss of cellular elongation and distinct cell borders, and increased vacuolization. The morphological characteristics of the FLCN-deleted cells resembled those of LPS-stimulated cells (Figure 4A, right). Consistent with these visual observations, quantitative flow cytometry showed that FLCN-deleted BMDMs displayed increased granularity and size (Figure 4B), as well as increased surface expression of CD80 (Figure 4C), reflecting an enhanced baseline activation status compared with that of control cells. Furthermore, real-time qPCR analysis revealed that FLCN deletion strongly decreased the expression of M2 surface marker arginase I (Arg1) and C-type lectin domain family 10 (Clec10a) under IL-4 stimulation (Figure 4D), indicating that FLCN deficiency promotes spontaneous M1-type activation in BMDMs.

We next tested the effects of inflammatory stimulation on FLCN-KO cells. Morphological changes induced by LPS in BMDMs were markedly accentuated in the absence of FLCN (Figure 4B), leading to a synergistic increase in surface CD80 expression and, most strikingly, surface class II MHC expression (Figure 4C). Cytokine and chemokine production is a hallmark of activated macrophages (27). To assess

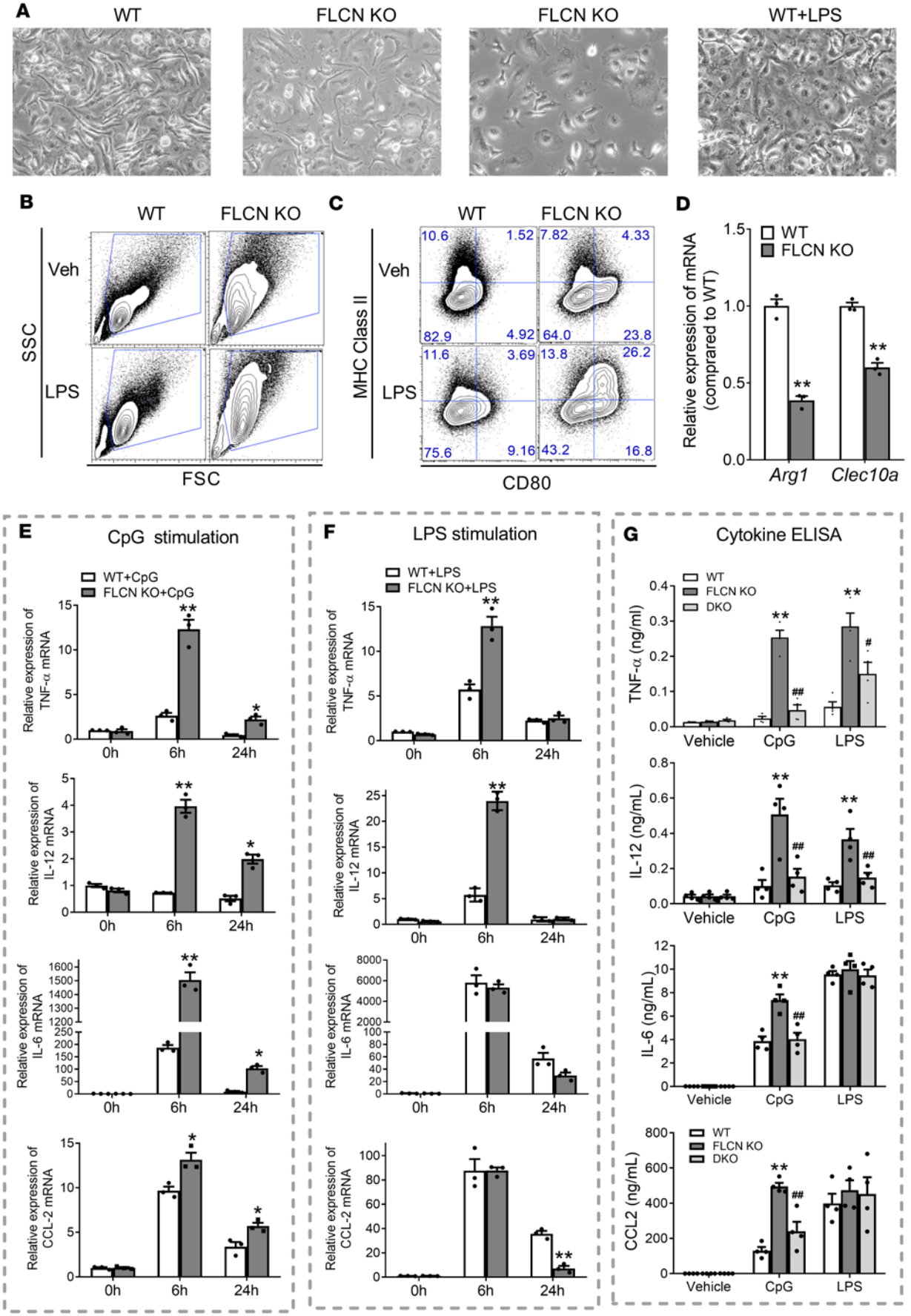
A
WT
FLCN KO
FLCN KO
WT+LPS
B
WT
FLCN KO
Veh
LPS
SSC
FSC
C
WT
FLCN KO
Veh
LPS
MHC Class II
CD80
10.6
1.52
82.9
4.92
7.82
4.33
64.0
23.8
11.6
3.69
75.6
9.16
13.8
26.2
43.2
16.8
D
WT
FLCN KO
Relative expression of mRNA (comprared to WT)
Arg1
Clec10a
E
CpG stimulation
WT+CpG
FLCN KO+CpG
Relative expression of TNF-α mRNA
Relative expression of IL-12 mRNA
Relative expression of IL-6 mRNA
Relative expression of CCL-2 mRNA
0h
6h
24h
F
LPS stimulation
WT+LPS
FLCN KO+LPS
G
Cytokine ELISA
WT
FLCN KO
DKO
TNF-α (ng/ml)
IL-12 (ng/mL)
IL-6 (ng/mL)
CCL2 (ng/mL)
Vehicle
CpG
LPS

Figure 4. BMDMs lacking FLCN are hypersensitive to LPS and CpG stimuli. (**A**) Bright-field images (original magnification, ×200) of BMDMs isolated from FLCN$^{lox/lox}$ (WT) and FLCN$^{lox/lox}$ Lyz2 Cre (FLCN KO) mice. (**B**) Forward scatter (FSC) and side scatter (SSC) characteristics of WT and FLCN KO BMDMs treated with vehicle (Veh) or LPS (100 ng/ml) for 24 hours. (**C**) Class II MHC and CD80 expression of WT and FLCN-KO BMDMs treated with vehicle or LPS for 24 hours was analyzed by flow cytometry. Graphs represent the percentage of the population. (**D**) Relative mRNA expression of M2 markers, *Arg1* and *Clec10a*, in WT and FLCN-KO BMDMs stimulated with IL-4 (10 ng/ml) for 24 hours. Values are represented as mean ± SEM from 3 independent experiments. $^{**}P <$ 0.01 vs. WT, determined by Student's *t* test. (**E** and **F**) Relative mRNA expression of *Tnf-α*, *Il-6*, *Il-12*, and *Ccl2* from WT and FLCN-KO BMDMs stimulated with CpG (10 μg/ml) or LPS (100 ng/ml) for 0, 6, and 24 hours. Values are represented as mean ± SEM from 3 independent experiments. $^{*}P < 0.05$, $^{**}P <$ 0.01 vs. WT, determined by Student's *t* test. (**G**) Secreted TNF-α, IL-6, IL-12, and CCL2 levels measured by ELISA in BMDMs isolated from WT, FLCN-KO, and FLCN$^{lox/lox}$ Lyz2 Cre TFE3-KO (DKO) mice, stimulated with vehicle, CpG, or LPS for 24 hours. Values are represented as mean ± SEM from 4 independent experiments. $^{**}P < 0.01$ vs. WT, $^{\#}P < 0.05$ $^{\#\#}P < 0.01$ vs. FLCN KO, determined by 1-way ANOVA followed by *t* test (Bonferroni correction).

the effect of FLCN deletion on secretion of cytokines and chemokines, WT and FLCN-KO BMDMs were stimulated with CpG or LPS for 24 hours. The production and secretion of numerous cytokines, in response to either CpG or LPS stimulation, was enhanced in FLCN-deleted cells compared with WT cells, including key mediators of inflammatory responses, such as granulocyte colony–stimulating factor (G-CSF), TNF-α, IL-6, soluble intercellular adhesion molecule-1 (sICAM-1), and macrophage inflammatory protein 1-α (chemokine [C-C motif] ligand 3 [CCL3]) (Supplemental Figure 2). qPCR studies demonstrated marked induction of numerous cytokine and chemokine genes in FLCN-KO BMDMs under CpG or LPS stimulation, including *Tnf-α*, *Il-6*, *Il-12*, and *Ccl2* (Figure 4, E and F). ELISAs confirmed the marked increase in cytokine secretion by BMDMs lacking FLCN (Figure 4G).

These data suggested that FLCN regulates BMDM activation in part via TFE3-mediated regulation of the expression of cytokine genes. To test this notion, BMDMs lacking *both* FLCN and TFE3 were stimulated with LPS or CpG. As shown in Figure 4G, deletion of TFE3 nearly completely abolished the procytokine secretion effects of FLCN deletion. Together, these data demonstrate that FLCN regulates both baseline and stimulated primary macrophage activation, as well as cytokine production, and that a large part of this regulation occurs via TFE3-mediated regulation of cytokine gene expression.

Loss of FLCN in monocyte lineage leads to expansion of peripheral monocyte progenitors via TFE3. Activation of monocytes in vivo leads to their proliferation and expansion (27). To test the role of myeloid FLCN in vivo, we generated mice lacking FLCN in the myeloid lineage, using Lyz2-Cre drivers (FLCN myeloid KO). The mice did not show any gross phenotype at the age of 2–3 months (data not shown). Myeloid progenitor numbers and mature cell numbers were quantified by flow cytometry in peripheral tissues, including spleen (Figure 5A) and liver (Figure 5B), and in bone marrow (Figure 5C). Strikingly, there was a remarkable expansion of progenitors (GMPs, CMPs, and common monocyte progenitors [cMoPs]) in peripheral tissues but not in bone marrow. Neutrophil and macrophage numbers were also increased in peripheral tissues. Coinciding with myeloid expansion, the spleen weight increased significantly, and liver weight tended to increase in FLCN myeloid KO mice (Figure 5D). Spleen histology assessed by H&E staining revealed disorganized ultrastructure, and macrophage infiltration within the red pulp, in FLCN myeloid KO mice (Figure 5E). Consistent with expansion of myeloid progenitors, peripheral blood monocytes were elevated in FLCN myeloid KO mice versus controls (0.46 ± 0.02 vs. 0.13 ± 0.02, $P < 0.01$), while other complete blood cell indices showed no differences. Strikingly, all of these observed phenotypes were reversed by codeletion of TFE3 (Figure 5, A–D), indicating that the activation of TFE3 by loss of FLCN mediates the marked expansion of progenitors. Myeloid loss of FLCN thus leads to progenitor expansion and neutrophil/macrophage infiltration in peripheral tissues via activation of TFE3.

Myeloid FLCN deletion evokes systemic histiocytic inflammation in a TFE3-dependent manner. To determine what tissues would be affected by prolonged activation of monocytes, we allowed FLCN myeloid KO mice to age up to 12 months old. By approximately 8 months of age, FLCN myeloid KO mice displayed mild and patchy alopecia (data not shown). Complete blood cell analysis indicated the development of anemia in these mice, with significantly reduced red blood cell counting, hemoglobin concentration, and low hematocrit (Table 1). In addition, the number of monocytes significantly increased while eosinophils and basophils markedly decreased in the peripheral blood of FLCN myeloid KO mice. By 12 months of age, FLCN myeloid KO mice exhibited marked and diffuse alopecia, extending from the rostral ear margin (including the top of head) to the tail base, with only small patches of hair remaining over the perineum and distal limbs (Figure 6A). Mice were sacrificed at this point, and tissues were dissected, revealing dramatically enlarged spleens and livers in FLCN myeloid KO mice (Figure 6B). Tissue histology, assessed by H&E staining, revealed profound multiorgan infiltration of histiocytes/macrophages

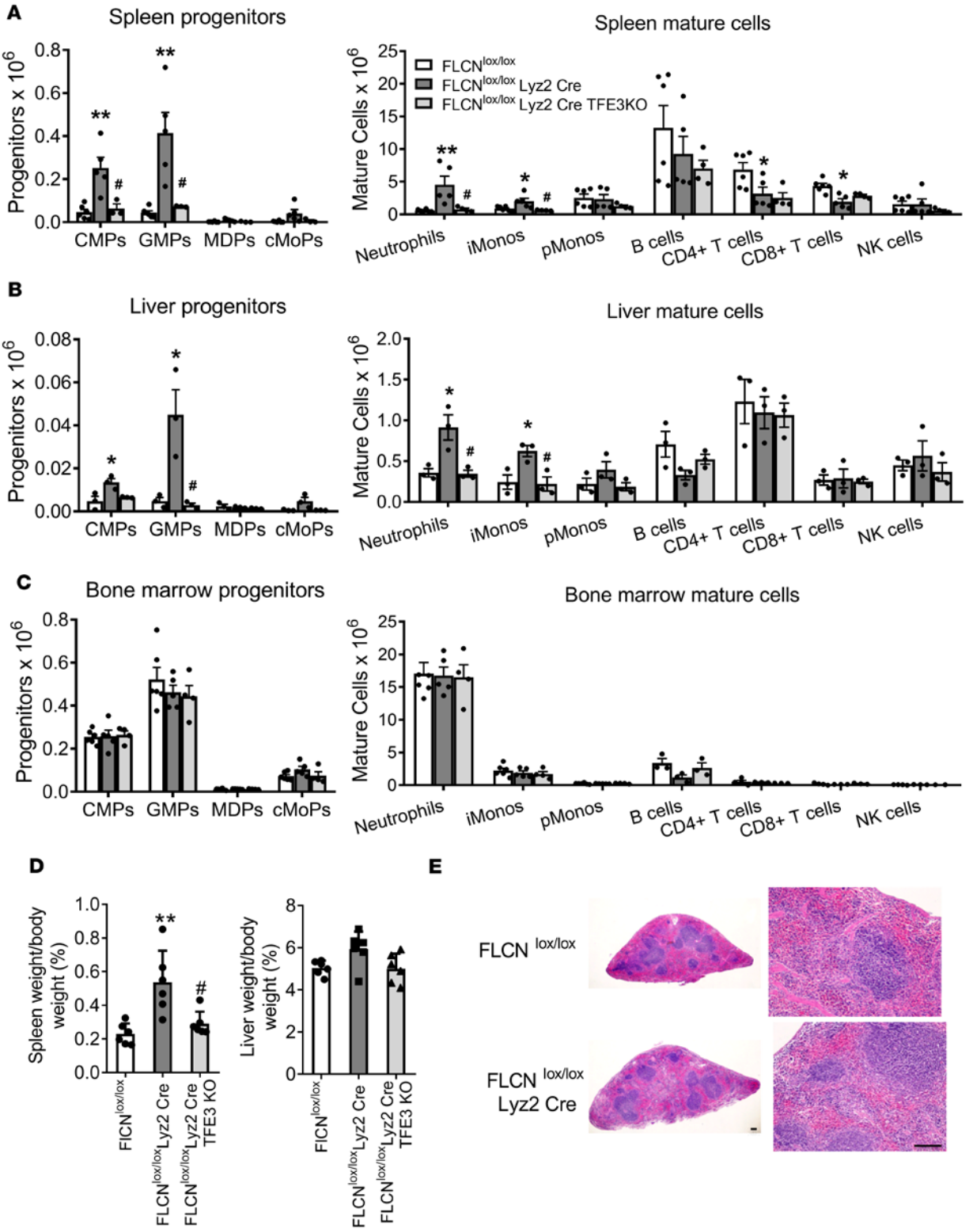

Figure 5. Loss of FLCN in monocyte lineage leads to expansion of peripheral monocyte progenitors via TFE3. (**A–C**) Progenitor and mature cell counting by FACS in spleens, livers, and bone marrow isolated from 12-week-old FLCN$^{lox/lox}$, FLCN$^{lox/lox}$ Lyz2 Cre, and FLCN$^{lox/lox}$ Lyz2 Cre TFE3 KO mice. Values are represented as mean ± SEM from 3–6 animals per group. *$P < 0.05$, **$P < 0.01$ vs. FLCN$^{lox/lox}$, #$P < 0.05$ vs. FLCN$^{lox/lox}$ Lyz2 Cre, determined by 1-way ANOVA followed by *t* test (Bonferroni correction). (**D**) Spleen weight/body weight (percentage) and liver weight/body weight (percentage) were calculated from 6 animals for each genotype at 12 weeks of age. Data are represented as mean ± SEM. **$P < 0.01$ vs. FLCN$^{lox/lox}$, #$P < 0.05$ vs. FLCN$^{lox/lox}$ Lyz2 Cre, determined by 1-way ANOVA followed by *t* test (Bonferroni correction). (**E**) H&E staining of spleens from 8-week-old FLCN$^{lox/lox}$ and FLCN$^{lox/lox}$ Lyz2 Cre mice. Scale bar: 200 μm.

in FLCN myeloid KO mice, including spleen, bone marrow, skin, liver, lymph node, and inguinal white adipose tissue (Figure 6C and Supplemental Figure 3). The infiltrating macrophages were large and round, with extensive eosinophilic cytoplasm, hallmarks of activated macrophages. The macrophages in the spleen, liver, and bone marrow frequently contained phagocytosed red blood cells along with yellow-brown pigment (Supplemental Figure 3), likely representing the blood breakdown product hemosiderin. This extensive erythrophagocytosis may explain the observed significant anemia. F4/80 (EMR1) is a heavily glycosylated G protein–coupled receptor and is a well-established marker for mouse macrophages. F4/80 staining indicated profound macrophage infiltration in all analyzed tissues of FLCN myeloid KO mice. In the liver, F4/80 positively stained macrophages formed multifocal aggregates, akin to hepatic granulomas. In the skin, the dermis and subcutaneous fat were expanded by numerous macrophages, displacing hair follicles and likely explaining the alopecia. In the spleen, there was extensive macrophage infiltration within the red pulp and, to a slightly lesser extent, white pulp. Strikingly, once again, all of these gross and histological abnormalities were completely reversed by concomitant genetic deletion of TFE3 (Figure 6), demonstrating that FLCN regulates macrophage/monocyte biology largely via the modulation of TFE3 activity. Collectively, our data demonstrate that activation of myeloid TFE3 by the loss of FLCN induces profound systemic histiocytic inflammation.

Discussion

We define here the role of FLCN in myeloid cells as a key modulator of mTORC1 activation, conferring specificity to mTORC1 regulation of lysosomal biogenesis and cytokine production and mediating LPS-induced activation of macrophages.

The role of mTOR in innate immunity and macrophage activation is complex. Numerous studies support the notion that mTOR activity in macrophages suppresses inflammatory responses. For example, treating macrophages with rapamycin increases the secretion of inflammatory cytokines (28). Myeloid disruption of LAMTOR1, an essential component of the amino acid–sensing pathway to mTORC1, results in M1 polarization of macrophages, thus leading to histiocytic inflammation (25, 26). On the other hand, and in seeming contradiction, LPS and other inflammatory activators powerfully activate mTOR signaling, which is required for a full inflammatory response (29, 30). Our work begins to resolve these paradoxes by demonstrating that FLCN confers specificity to the mTOR response. LPS stimulates canonical mTOR signaling to S6K and other substrates while simultaneously suppressing mTOR signaling to TFE3 by virtue of suppressing FLCN (Figure 7). mTORC1 signaling thus has both activating and suppressing effects on macrophage inflammatory responses, and FLCN allows LPS to coordinate activation of the former and suppression of the latter.

FLCN was originally identified as a tumor suppressor gene, mutated in the familial hamartomatous syndrome, Birt-Hogg-Dube syndrome (11, 31). Paradoxically, however, tumors in these patients invariably contain hyperactive mTORC1, rather than suppressed activity as would be expected from the loss of activation of RagC/D, a key mTORC1-activating G protein. Our data not only demonstrate that, in the absence of FLCN, canonical mTORC1 activity is not suppressed, but also explain why mTORC1 activity is in fact increased: the loss of TFE3 phosphorylation leads to its nuclear translocation and dramatic induction of RagD gene expression, thus increasing RagD availability for the mTORC1 complex, leading to stimulation of canonical mTORC1 to S6K and other substrates. This RagD feedback loop likely contributes to neoplastic proliferation in Birt-Hogg-Dube patients, providing a potentially novel target in these patients.

TFE3 and TFEB are increasingly recognized as key regulators of the inflammatory response in macrophages. The pathway is evolutionarily distant, with even the TFE3 and TFEB homolog HLH-30 in *C. elegans* essential for host defense upon bacterial infection (32). In mammals, exposure of macrophages to bacteria, antibody-coated particles, or bacterial antigens, such as LPS promotes nuclear localization of TFE3 and TFEB (23). However, how LPS promotes nuclear localization of TFE3 and TFEB was not clear. Our data demonstrate that the activation of TFE3 is mediated in large part via suppression of FLCN by LPS. TFE3 and TFEB can then engage a large gene network in macrophages, including, most notably, a program of lysosomal biogenesis and a program of cytokines and chemokines (14, 23, 33), both of which are critical for efficient eradication of infection. Certain chronic infections, such as tuberculosis, persist in part by suppressing host myeloid immunity and may benefit from activation of the TFE3/TFEB pathway. Targeting FLCN may thus represent a novel approach to reactivate myeloid function and eradicate infection in such indolent disease.

Table 1. Complete blood cell analysis of peripheral blood from FLCN$^{lox/lox}$, FLCN$^{lox/lox}$ Lyz2 Cre, and FLCN$^{lox/lox}$ Lyz2 Cre TFE3-KO mice at 8 months old

	FLCN$^{lox/lox}$	FLCN$^{lox/lox}$ Lyz2 Cre	FLCN$^{lox/lox}$ Lyz2 Cre TFE3 KO
RBC (×10^6/μl)	*10.93 ± 0.50*	*7.96 ± 0.63*^{A}	*10.59 ± 0.63*^{B}
Hemoglobin (g/dl)	15.96 ± 0.55	11.78 ± 0.75^A	15.46 ± 0.67^B
Hematocrit (%)	51.02 ± 2.24	36.81 ± 2.39^A	49.73 ± 2.18^B
MCV (fl)	46.76 ± 0.61	46.77 ± 1.28	47.35 ± 1.14
MCH (pg)	14.67 ± 0.20	14.96 ± 0.33	14.72 ± 0.34
MCHC (g/dl)	31.40 ± 0.45	32.03 ± 0.42	31.14 ± 0.61
RDW (%)	27.02 ± 0.31	25.15 ± 0.89	26.42 ± 1.55
WBC (×10^3/μl)	9.18 ± 0.70	7.86 ± 0.48	9.52 ± 0.64
Neutrophils (×10^3/μl)	1.40 ± 0.10	1.21 ± 0.11	1.51 ± 0.23
Lymphocytes (×10^3/μl)	7.34 ± 0.66	5.92 ± 0.40	7.27 ± 0.54
Monocytes (×10^3/μl)	0.25 ± 0.03	0.59 ± 0.05^A	0.29 ± 0.03^C
Eosinophils (×10^3/μl)	0.13 ± 0.02	0.12 ± 0.02	0.17 ± 0.04
Basophils (×10^3/μl)	0.05 ± 0.02	0.03 ± 0.01	0.03 ± 0.01
Platelets (×10^3/μl)	1030.19 ± 45.43	855.94 ± 32.86	961.86 ± 64.15

Values are presented as mean ± SEM. One-way ANOVA was performed, followed by a *t* test (Bonferroni correction). $n = 8$ per group. $^AP < 0.01$ vs. FLCN$^{lox/lox}$; $^BP < 0.05$, $^CP < 0.01$ vs. FLCN$^{lox/lox}$ Lyz2 Cre. RBC, red blood cell; MCV, mean corpuscular volume; MCH, mean corpuscular hemoglobin; MCHC, mean corpuscular hemoglobin concentration; RDW, red cell distribution width; WBC, white blood cells.

Importantly, innate inflammatory processes must also be dialed down once infection has resolved or been controlled. Our data demonstrate the consequences of insufficiently downregulated macrophage activation, i.e., marked myeloid expansion and pronounced diffuse histiocytic infiltration. Fortunately, this process appears to be very slow, potentially allowing for short-to-medium-term FLCN-directed therapy. Of note, however, Baba et al. reported that acute loss of FLCN in hematopoietic stem cells leads to bone marrow failure and death in 40 days (20), indicating that any FLCN therapy would have to either be targeted to monocytes or titrated accordingly. Also of note, in the same study, hyper mTORC1 activity was noted in HSCs, for which we provide the likely explanation here: activation of the TFE3-induced RagD feedback loop.

Our epistatic experiments clearly demonstrate that TFE3 is absolutely required for the marked activation of macrophages elicited by suppression of FLCN in cell culture as well as the diffuse histiocytic infiltration observed in vivo with FLCN deletion. Our data thus indicate that TFE3 and TFEB are not redundant in myeloid cells. TFE3 and TFEB have overlapping, though not identical, gene targets, which may explain the necessity of TFE3. Both factors are expressed in myeloid cells, but TFE3 may perhaps be the dominant regulator in these cells. Alternatively, TFE3 and TFEB may form obligate heterodimers, although the existence of such complexes has been questioned (34). Testing if TFEB is also necessary for the effects seen with inhibition of FLCN will be of future interest.

The phenotype of the FLCN myeloid KO mouse recapitulates some of the hallmarks of histiocytic syndromes, including Erdheim-Chester disease (ECD). Much like in patients with ECD, presentation does not occur until a late age. No mutations in FLCN have been noted in ECD, which has been predominantly characterized by somatic activating mutations in the Ras/Erk pathway. However, given the rarity of the disease, a role of FLCN cannot be ruled out by a lack of genetic data at this point in time. Germline mutations would almost certainly be unlikely because systemic mutations in FLCN confer significant evolutionary disadvantages in other tissues. Indeed, FLCN total body KO animals are not viable (35). Nevertheless, epigenetic or other suppression of FLCN may be an important component of these diseases, even in the absence of somatic mutations. The fact that the mTOR inhibitor sirolimus showed efficacy in ECD (36) suggests that activation of this pathway may indeed be relevant, and future studies of ECD genetics might focus on FLCN and TFE3, particularly in the subset of patients without BRAF mutations.

In summary, our work identifies a critical role for FLCN in modulation of the mTORC1 pathway in myeloid cells; demonstrates the existence of specific subbranches of mTORC1 signaling that affect

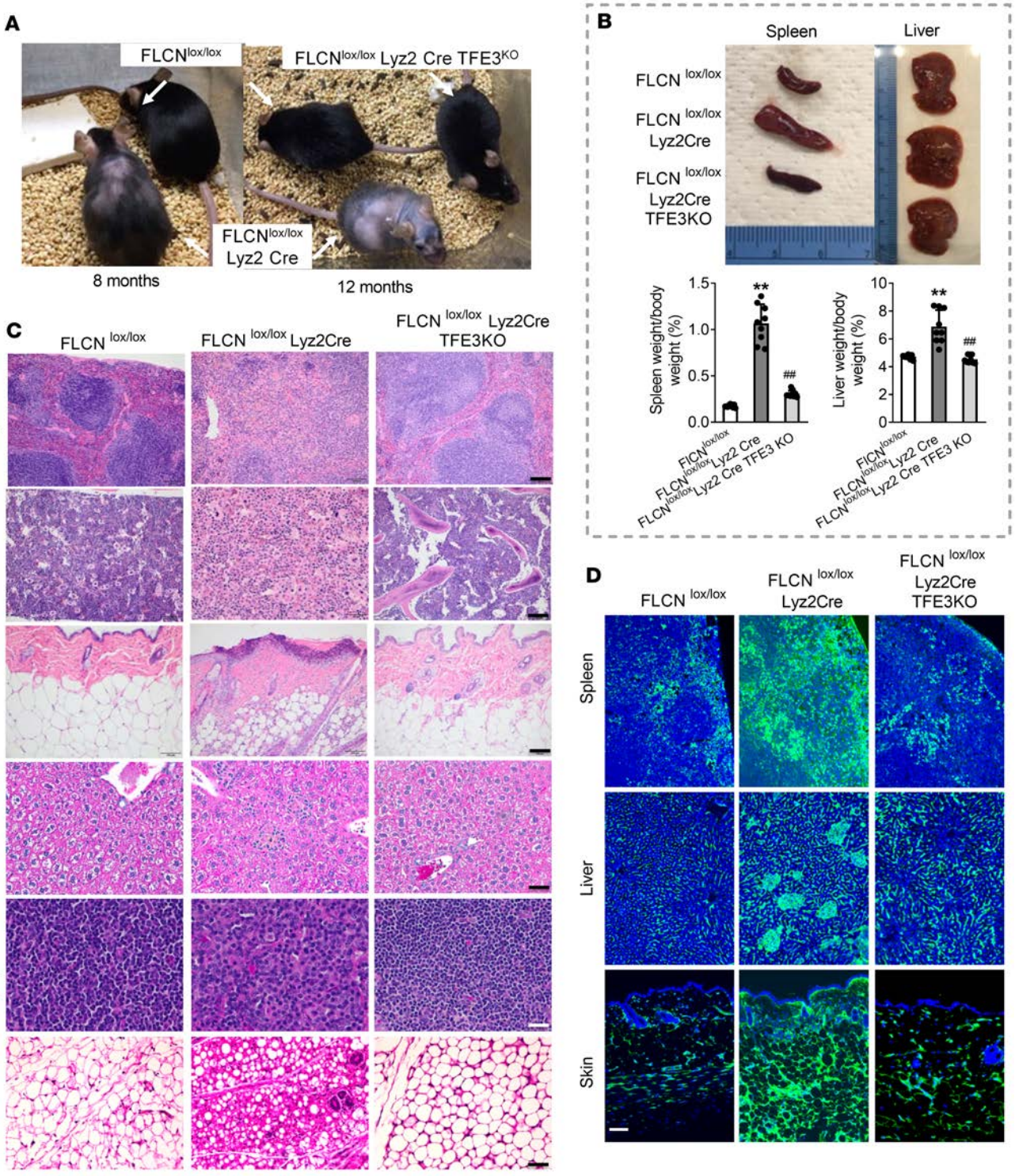

Figure 6. Myeloid FLCN inactivation leads to systemic histiocytic inflammation in mice, which is largely rescued by TFE3 deletion. (**A**) Gross images of FLCN$^{lox/lox}$, FLCN$^{lox/lox}$ Lyz2 Cre, and FLCN$^{lox/lox}$ Lyz2 Cre TFE3 KO mice at 8 and 12 months old. (**B**) Gross images of spleens and livers from 12-month-old mice of different genotypes. Data are represented as mean ± SEM from 9 animals for each genotype. $^{**}P < 0.01$ vs. FLCN$^{lox/lox}$, $^{\#\#}P < 0.05$ vs. FLCN$^{lox/lox}$ Lyz2 Cre, determined by 1-way ANOVA followed by *t* test (Bonferroni correction). (**C**) H&E staining of spleens, bone marrow, skin, livers, lymph nodes, and inguinal white adipose tissue (iWAT) from 12-month-old mice of different genotypes. Hemophagocytosis was indicated by black arrow. Black scale bar: 100 μm. White scale bar (lymph node): 50 μm. (**D**) F4/80 staining (green) and DAPI (blue) in the spleens, livers, and skin from 12-month-old mice of different genotypes. Scale bar: 200 μm.

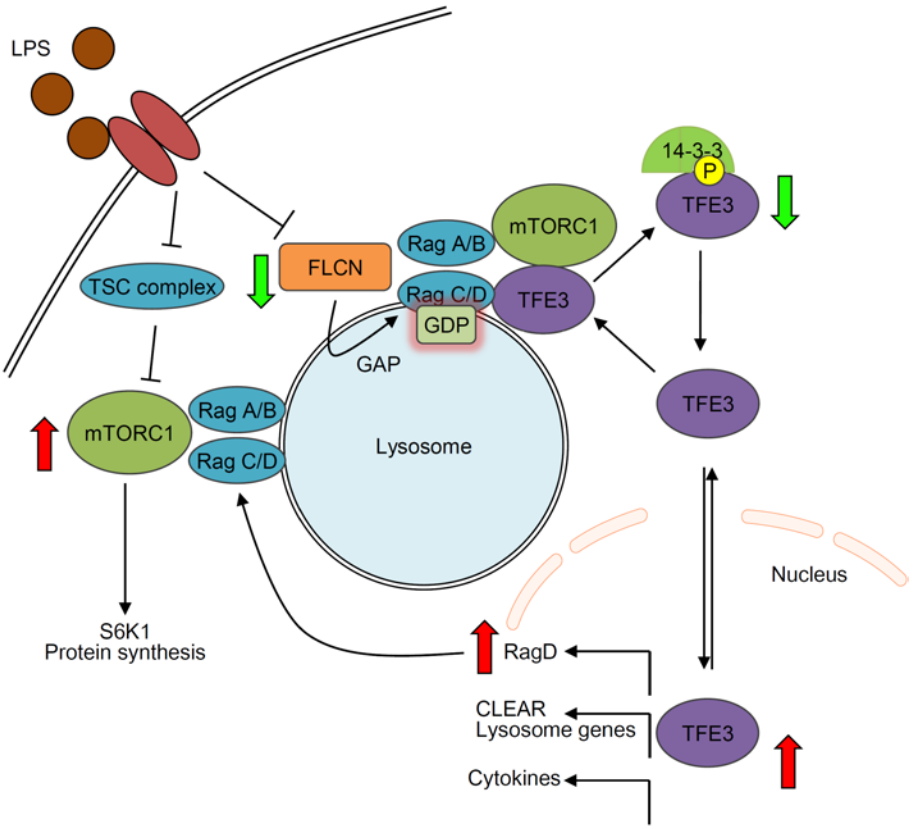

Figure 7. Model of how LPS specifically modulates different arms of mTOR signaling. LPS activates canonical mTORC1/S6K signaling, likely in large part via suppression of the TSC complex, while suppression of FLCN by LPS specifically suppresses noncanonical mTORC1/TFE3 signaling. Subsequent nuclear translocation of TFE3 activates expression of the lysosome biogenesis program, of cytokine transcription, and of RagD. Expression of RagD forms a feedback loop, leading to hyperactivation of canonical (non-FLCN requiring) mTOR activity.

inflammatory signaling differently; provides a mechanism by which LPS promotes TFE3 nuclear translocation and lysosome biogenesis; and illustrates the effects of chronic low-grade macrophage activation in vivo. The work thus elucidates fundamental aspects of myeloid biology.

Methods

Animals. FLCN-floxed animals (17) were crossed with Lyz2-Cre mice (from Jackson Laboratory) to obtain FLCN myeloid-specific KO animals. TFE3-deficient animals (37) were bred to FLCN myeloid KO mice to obtain FLCN TFE3 double-KO animals. All animal experiments were littermate controlled and were performed on C57B6 and FVB or 129 mixed strains. Mice were housed in 12-hour light and dark cycles and fed with standard rodent diets or special diets if specified.

Antibodies. Phospho-TFE3 (Ser320) antibody was a gift and has been described (23). Other antibodies used were as follows: TFE3 (MilliporeSigma, HPA023881), FLCN (Abcam, ab124885), LAMP2 (Abcam, ab13524), HA tag (Cell Signaling Technology, 2367), β-actin (Cell Signaling Technology, 4970), phospho-p70S6K (Thr389) (Cell Signaling Technology, 9234), total p70S6K (Cell Signaling Technology, 2708), phospho-S6 ribosomal protein (Ser240/244) (Cell Signaling Technology, 2215), total S6 ribosomal protein (Cell Signaling Technology, 2217), phospho-mTOR (Ser2448) (Cell Signaling Technology, 5536), mTOR (Cell Signaling Technology, 2983), and RagD (Abcam, ab187679).

Complete blood cell analysis. The blood samples were collected with lavender top collection tubes containing EDTA, sent to the Pennsylvania Veterinary Laboratory, and analyzed using a hematology analyzer at times up to 24 hours after blood collection.

Isolation and processing of organs. Bone marrow cells were removed from the leg bones of mice by flushing the bone marrow cavity with cold PBS and filtering the cells over a 70-μm Falcon cell strainer. Spleens were

removed and weighed for analysis of splenomegaly. Splenocytes were harvested from whole spleens after digestion in DNase I (Roche) and collagenase (Roche) at 37°C for 30 minutes. Spleen digests were filtered over a 70-μm strainer. Liver leukocytes were harvested by filtering the bulk liver through a 70-μm strainer. After centrifugation, the liver cell pellet was resuspended in 30% Percoll and layered over 70% Percoll prior to being spun at room temperature at 1000 *g* for 20 minutes. The liver leukocytes were harvested at the Percoll interface. After the tissue and blood cells were harvested, red blood cell lysis was performed using ACK lysis buffer from Lonza prior to cell counting. Cells were counted on a Countess Automated Cell Counter from Thermo Fisher Scientific to calculate the number of cells harvested from each organ. The cells were then placed in culture or subjected to cell surface marker immunofluorescence staining for FACS analysis.

Cellular immunophenotyping. Fluorescently labeled cells were analyzed on a BD LSRII or Miltenyi MacsQuant. FACS data were analyzed using FlowJo software, which was used to create all flow cytometry plots. All populations were gated on forward and side scatter to limit inclusion of dead cells, debris, and doublets. Live cells were identified by excluding cells staining positive for Live-Dead reagents obtained from Thermo Fisher Scientific. Inflammatory monocytes were identified as $Ly6G^-Ly6C^+Ccr2^+$ or $Ly6G^-Ly6C^+CD115^+$ cells. Myeloid progenitors were identified as CMPs ($Lin^-cKit^+CD105^-CD16/32^{lo}CD115^-$), GMPs ($Lin^-cKit^+CD105^-CD16/32^{hi}CD115^-$), MDPs ($Lin^-cKit^+CD105^-CD115^{hi}Ly6C^-$), or cMoPs ($Lin^-cKitCD105^-CD115^{hi}Ly6C^+$). The lineage panel included antibodies against B220, CD4, CD5, CD8a, CD11b, CD11c, CD90.2, DX5, Ly6G, NK1.1, and Ter119. The following fluorescently labeled antibodies were used: PE anti-mouse B220 antibody (clone RA3-6B2) (Biolegend, 103207), PE anti-mouse CD4 antibody (clone RM4-5) (BD Biosciences, 553049), PE anti-mouse CD5 antibody (clone 53-7.3) (BD Biosciences, 553023), PE anti-mouse CD8a antibody (clone 53-6.7) (Biolegend, 100708), APC/Cy7 anti-mouse CD11b antibody (clone M170) (BD Biosciences, 557657), PE anti-mouse CD11b antibody (clone M170) (eBiosciences, 12-0112-82), PE anti-mouse CD11c antibody (clone HL3) (BD Biosciences, 557401), APC/Cy7 anti-mouse CD16/32 antibody (clone 93) (Biolegend, 101328), PE anti-mouse CD49b antibody (clone DX5) (Biolegend, 108908), PE anti-mouse CD90.2 antibody (clone 53-2.1) (BD Biosciences, 553006), PerCP/Cy5.5 anti-mouse CD105 antibody (clone MJ7/18) (Biolegend, 120416), APC anti-mouse CD115 antibody (clone AFS98) (eBiosciences, 17-1152-82), PE/Cy7 anti-mouse CD115 antibody (clone AFS98) (eBiosciences, 25-1152-82), APC anti-mouse Ccr2 antibody (clone 475301) (R&D Systems, FAB5538A-100), PE anti-mouse Ccr2 antibody (clone 475301) (R&D Systems, FAB5538P-100), APC anti-mouse c-Kit/CD117 antibody (clone 2B8) (BD Biosciences, 553356), PE anti-mouse GR-1 antibody (clone RB6-8C5) (Biolegend, 108408), PE anti-mouse IL-12 (p40/p70) antibody (clone C15.6) (BD Biosciences, 554479), PacBlue anti-mouse Ly6C antibody (clone HK1.4) (Biolegend, 128014), FITC anti-mouse Ly6G antibody (clone 1A8) (BD Biosciences, 561105), PE anti-mouse Ly6G antibody (clone 1A8) (BD Biosciences, 551461), PE anti-mouse NK1.1 antibody (clone PK136) (Biolegend, 108708), PE-Cy7 anti-mouse pSTAT1 (clone A15158B) (Biolegend, 686408), PE anti-mouse Sca-1 antibody (clone D7) (Biolegend, 108108), and PE anti-mouse Ter119 antibody (clone TER-119) (Biolegend, 116208).

Cell culture. For preparation of BMDMs, mice were killed by cervical dislocation, and the femur and tibia of the hind legs were dissected and bone marrow cavities were flushed with 5 ml cold, sterile PBS. After lysing red blood cells, the bone marrow cells were washed, resuspended, and differentiated into BMDMs in DMEM with 10% FBS, 10% L929 conditioned medium, 100 μg/ml streptomycin, and 100 U/ml penicillin. Six days after initial BMDMs cell culture, the purity of $F4/80^+$ cells was >90%, as determined by flow cytometry. L-929 cells (ATCC, CCL-1) were grown in DMEM with GlutaMAX and sodium pyruvate (Gibco, 10569-044) supplemented with 1% fetal bovine serum for 1 week, and the medium was filtered using a 0.22-μm filter and stored at –20°C. RAW 264.7 (ATCC, TIB-71) were grown in DMEM with GlutaMAX and sodium pyruvate (Gibco, 10569-044) supplemented with 10% fetal bovine serum. RAW cells and BMDM cells were stimulated with vehicle (PBS), 10 μg/ml CpG 1826 or 100 ng/ml LPS from *Escherichia coli* 0111:B4 (MilliporeSigma, L4391). The class B CpG1826 oligonucleotide was synthesized by Integrated DNA Technologies. Cell culture supernatants were collected for cytokine detection by BD OptEIA ELISA sets (BD Biosciences) following the manufacturer's instructions.

Plasmids, transfection, and virus vector production. FLCN-HA or TFE3 cDNA was transferred to pLenti CMV Puro DEST (a gift from Eric Campeau, Program in Gene Function and Expression, University of Massachusetts Medical School, Worcester, Massachusetts, USA) (Addgene, plasmid 17452). Amino acid sequences surrounding S320 were as follows (the serine residue or substituted alanine residue is under-

lined): TFE3 WT (TPAITVSNSCPAELPNIK) and TFE3 S320A (TPAITVSNACPAELPNIK). Lenti transfer plasmid psPAX2 (a gift from Didier Trono, School of Life Sciences, EcolePolytechnique Federale de Lausanne, Lausanne, Switzerland) (Addgene, plasmid 12260) and pMD2.G (a gift from Didier Trono) (Addgene, plasmid 12259) were cotransfected to HEK293T cells by Fugene HD (Promega). Seventy-two hours later, supernatant was harvested and cell debris was removed by a low-protein-binding 0.45-μm syringe filter. Virus particles containing supernatant were stored at −80°C until use. For lenti or retroviral infection, the spinfection method was used. Cells were plated on 6-well multiwell plates, and 2 ml virus containing supernatant and 2 ml fresh medium were added per well. Polybrene was added to medium with a final concentration of 8 μg/ml. A 6-well plate was centrifuged at 1000 *g* for 1.5 hour (spinfection), and then the medium was replaced with fresh medium. Drug selection with the appropriate marker was started 24–48 hours after the spinfection.

Gene editing by the CRISPR/Cas9 system. The protocol distributed by the Zhang laboratory at Massachusetts Institute of Technology was used. lentiCRISPR version 2 was a gift from Feng Zhang (Department of Biological Engineering, Massachusetts Institute of Technology, Cambridge, Massachusetts, USA) (Addgene, plasmid 52961). Guide RNAs (gRNAs) specific to genes of interests were designed by using a web-based algorithm from the Zhang laboratory (Optimized CRISPR Design; http://crispr.mit.edu). Briefly, gRNA was designed as close to the start codon as possible, and the top 1 or 2 candidates were picked up and validated by Western blot. The gRNA sequence was as follows (the pam sequence is excluded): mouse nontarget control (5′-ATTGTTCGACCGTCTACGGG-3′), mouse flcn (5′-GAGCCCTTGGTGAGTCCATA-3′). Cells were infected with lentivirus encoding for CAS9/gRNA, followed by puromycin selection, and used as populations.

Western blot analysis. Tissue or cell samples were lysed by RIPA buffer containing phosphatase inhibitor (PhosSTOP, Roche) and proteinase inhibitor (Complete miniproteinase inhibitor cocktail, Roche). Samples were sonicated followed by centrifugation to remove insoluble debris or lipid. Protein concentration was quantified by the BCA protein assay kit (Thermo Fisher Scientific), and the same amount of protein (10–20 μg) was loaded to 4%–20% gradient Tris-glycine polyacrylamide gel (Bio-Rad) and electrophoresed (SDS-PAGE). After the SDS-PAGE, protein samples were transferred to PVDF membrane (MilliporeSigma). Membranes were blocked with 5% skim milk for 1 hour and then incubated with the respective primary antibodies (see *Antibodies* above). Appropriate HRP-conjugated secondary antibodies were selected according to the host species of primary antibodies, and images were taken by using a digital imager (GE Healthcare Life Sciences, ImageQuant LAS 4000).

Gene expression analysis. mRNA expression was quantified by quantitative reverse transcription–PCR. Total RNA was extracted by using the TurboCapture mRNA kit (Qiagen) for cells. qPCR was performed by using the SYBR Green method (iQ SYBR Green super mix), and values were normalized to 36B4, Hprt, and Gapdh expression by the ΔΔCt method. Primer sequences are provided in Supplemental Table 1.

Histology analysis and immunofluorescence staining of cells. Isolated tissues were fixed in 3.7% formaldehyde for 24–48 hours followed by dehydration steps. Tissues were embedded in paraffin and sectioned, and then H&E staining was performed. Stained sections were examined under light microscope, and images were captured. Cells were plated on the glass slips coated with gelatin. Cells were fixed with 3.7% formaldehyde in PBS and permeabilized with 0.3% Triton X-100/PBS (PBST). Blocking and primary antibody incubation were performed in PBST containing 5% BSA overnight followed by secondary antibody incubation. Images of the cells were taken via confocal microscopy.

Statistics. Values are presented as mean ± SEM. Student's *t* test (2-tailed unpaired *t* test) was performed for single comparison. For the comparisons of the groups more than 3, 1-way ANOVAs were performed, followed by a 2-tailed *t* test (Bonferroni correction). $P < 0.05$ was considered significant.

Study approval. All mouse experiments were performed according to procedures approved by the University of Pennsylvania Institute for Animal Care and Use Committees.

Author contributions

JL, SW, and LKW designed and conducted the experiments, analyzed/interpreted the data, and wrote the manuscript. CB helped perform critical experiments and provided intellectual input for the experiments. EMB provided intellectual input for the study design, interpreted the data, and wrote the manuscript. ZA designed the study, interpreted the data, and wrote the manuscript.

Acknowledgments

We thank Rosa Puertollano from the NIH for providing phospho-TFE3 (Ser320) antibody. We thank Lan Cheng and Min Min Lu from the Histology and Gene Expression Core at the Cardiovascular Institute of Perelman School of Medicine, University of Pennsylvania, for immunohistochemistry and histology services. We thank Amy Durham and Liz Buza from Penn Vet Diagnostic lab for comprehensive pathology analysis. We thank Andrea Stout and Jasmine Zhao from the Cell and Developmental Biology Microscopy Core at University of Pennsylvania for the support on confocal imaging. JL is supported by the National Natural Science Foundation of China (31771265) and the National High Technology Research and Development Program of China (2014AA020542). SW is supported by Toyobo Biotechnology Foundation and the American Diabetes Association (1-16-PDF-117). ZA is supported by the NIH (DK107667).

Address correspondence to: Zoltan Arany, Perelman School of Medicine, University of Pennsylvania, TRC11-106, 3400 Civic Boulevard, Philadelphia, Pennsylvania 19104, USA. Phone: 215.898.3482; Email: zarany@pennmedicine.upenn.edu.

1. Saxton RA, Sabatini DM. mTOR signaling in growth, metabolism, and disease. *Cell*. 2017;168(6):960–976.
2. Sancak Y, et al. The Rag GTPases bind raptor and mediate amino acid signaling to mTORC1. *Science*. 2008;320(5882):1496–1501.
3. Sancak Y, Bar-Peled L, Zoncu R, Markhard AL, Nada S, Sabatini DM. Ragulator-Rag complex targets mTORC1 to the lysosomal surface and is necessary for its activation by amino acids. *Cell*. 2010;141(2):290–303.
4. Zoncu R, Bar-Peled L, Efeyan A, Wang S, Sancak Y, Sabatini DM. mTORC1 senses lysosomal amino acids through an inside-out mechanism that requires the vacuolar H(+)-ATPase. *Science*. 2011;334(6056):678–683.
5. Goberdhan DC, Wilson C, Harris AL. Amino acid sensing by mTORC1: intracellular transporters mark the spot. *Cell Metab*. 2016;23(4):580–589.
6. Inoki K, Li Y, Xu T, Guan KL. Rheb GTPase is a direct target of TSC2 GAP activity and regulates mTOR signaling. *Genes Dev*. 2003;17(15):1829–1834.
7. Bar-Peled L, Schweitzer LD, Zoncu R, Sabatini DM. Ragulator is a GEF for the rag GTPases that signal amino acid levels to mTORC1. *Cell*. 2012;150(6):1196–1208.
8. Bar-Peled L, et al. A Tumor suppressor complex with GAP activity for the Rag GTPases that signal amino acid sufficiency to mTORC1. *Science*. 2013;340(6136):1100–1106.
9. Tsun ZY, et al. The folliculin tumor suppressor is a GAP for the RagC/D GTPases that signal amino acid levels to mTORC1. *Mol Cell*. 2013;52(4):495–505.
10. Petit CS, Roczniak-Ferguson A, Ferguson SM. Recruitment of folliculin to lysosomes supports the amino acid-dependent activation of Rag GTPases. *J Cell Biol*. 2013;202(7):1107–1122.
11. Schmidt LS. Birt-Hogg-Dubé syndrome: from gene discovery to molecularly targeted therapies. *Fam Cancer*. 2013;12(3):357–364.
12. Hasumi H, et al. Regulation of mitochondrial oxidative metabolism by tumor suppressor FLCN. *J Natl Cancer Inst*. 2012;104(22):1750–1764.
13. Wada S, et al. The tumor suppressor FLCN mediates an alternate mTOR pathway to regulate browning of adipose tissue. *Genes Dev*. 2016;30(22):2551–2564.
14. Puertollano R, Ferguson SM, Brugarolas J, Ballabio A. The complex relationship between TFEB transcription factor phosphorylation and subcellular localization. *EMBO J*. 2018;37(11):e98804.
15. Martina JA, Chen Y, Gucek M, Puertollano R. MTORC1 functions as a transcriptional regulator of autophagy by preventing nuclear transport of TFEB. *Autophagy*. 2012;8(6):903–914.
16. Settembre C, et al. A lysosome-to-nucleus signalling mechanism senses and regulates the lysosome via mTOR and TFEB. *EMBO J*. 2012;31(5):1095–1108.
17. Baba M, et al. Kidney-targeted Birt-Hogg-Dube gene inactivation in a mouse model: Erk1/2 and Akt-mTOR activation, cell hyperproliferation, and polycystic kidneys. *J Natl Cancer Inst*. 2008;100(2):140–154.
18. Cash TP, Gruber JJ, Hartman TR, Henske EP, Simon MC. Loss of the Birt-Hogg-Dubé tumor suppressor results in apoptotic resistance due to aberrant TGFβ-mediated transcription. *Oncogene*. 2011;30(22):2534–2546.
19. Hasumi Y, et al. Folliculin (Flcn) inactivation leads to murine cardiac hypertrophy through mTORC1 deregulation. *Hum Mol Genet*. 2014;23(21):5706–5719.
20. Baba M, et al. Loss of folliculin disrupts hematopoietic stem cell quiescence and homeostasis resulting in bone marrow failure. *Stem Cells*. 2016;34(4):1068–1082.
21. Hong SB, Oh H, Valera VA, Baba M, Schmidt LS, Linehan WM. Inactivation of the FLCN tumor suppressor gene induces TFE3 transcriptional activity by increasing its nuclear localization. *PLoS One*. 2010;5(12):e15793.
22. Martina JA, et al. The nutrient-responsive transcription factor TFE3 promotes autophagy, lysosomal biogenesis, and clearance of cellular debris. *Sci Signal*. 2014;7(309):ra9.
23. Pastore N, et al. TFEB and TFE3 cooperate in the regulation of the innate immune response in activated macrophages. *Autophagy*. 2016;12(8):1240–1258.
24. Di Malta C, et al. Transcriptional activation of RagD GTPase controls mTORC1 and promotes cancer growth. *Science*. 2017;356(6343):1188–1192.
25. Kimura T, et al. Polarization of M2 macrophages requires Lamtor1 that integrates cytokine and amino-acid signals. *Nat Commun*. 2016;7:13130.
26. Hayama Y, et al. Lysosomal protein lamtor1 controls innate immune responses via nuclear translocation of transcription fac-

tor EB. *J Immunol*. 2018;200(11):3790–3800.
27. Shi C, Pamer EG. Monocyte recruitment during infection and inflammation. *Nat Rev Immunol*. 2011;11(11):762–774.
28. Weichhart T, et al. The TSC-mTOR signaling pathway regulates the innate inflammatory response. *Immunity*. 2008;29(4):565–577.
29. Ivanov SS, Roy CR. Pathogen signatures activate a ubiquitination pathway that modulates the function of the metabolic checkpoint kinase mTOR. *Nat Immunol*. 2013;14(12):1219–1228.
30. Weichhart T, Hengstschläger M, Linke M. Regulation of innate immune cell function by mTOR. *Nat Rev Immunol*. 2015;15(10):599–614.
31. Nickerson ML, et al. Mutations in a novel gene lead to kidney tumors, lung wall defects, and benign tumors of the hair follicle in patients with the Birt-Hogg-Dubé syndrome. *Cancer Cell*. 2002;2(2):157–164.
32. Visvikis O, et al. Innate host defense requires TFEB-mediated transcription of cytoprotective and antimicrobial genes. *Immunity*. 2014;40(6):896–909.
33. Sergin I, et al. Exploiting macrophage autophagy-lysosomal biogenesis as a therapy for atherosclerosis. *Nat Commun*. 2017;8:15750.
34. Fisher DE, Carr CS, Parent LA, Sharp PA. TFEB has DNA-binding and oligomerization properties of a unique helix-loop-helix/leucine-zipper family. *Genes Dev*. 1991;5(12A):2342–2352.
35. Hasumi Y, et al. Homozygous loss of BHD causes early embryonic lethality and kidney tumor development with activation of mTORC1 and mTORC2. *Proc Natl Acad Sci U S A*. 2009;106(44):18722–18727.
36. Gianfreda D, et al. Sirolimus plus prednisone for Erdheim-Chester disease: an open-label trial. *Blood*. 2015;126(10):1163–1171.
37. Steingrimsson E, et al. Mitf and Tfe3, two members of the Mitf-Tfe family of bHLH-Zip transcription factors, have important but functionally redundant roles in osteoclast development. *Proc Natl Acad Sci U S A*. 2002;99(7):4477–4482.